Ferroelectricity of Pyridinium Perchlorate, a Molecular Level Point of View

Danilo Vujosevic, Klaus Müller, and Emil Roduner*

Institut für Physikalische Chemie, Universität Stuttgart, Pfaffenwaldring 55, D-70569 Stuttgart, Germany

Received: January 24, 2006; In Final Form: March 15, 2006

The behavior of ferroelectric and thermodynamic parameters of pyridinium perchlorate ($PyClO_4$) was simulated based on experimental NMR data and properties of the individual constituting ions. Dynamic ^2H NMR spectroscopy was used to investigate the order−disorder character of ferroelectricity in $PyClO_4$. Quadrupole echo and inversion recovery experiments were performed in the range from 140 to 300 K. The spectra can be simulated by a rotational jump motion of the pyridinium cations about their pseudo-C_6 axis. This confirms that the ferroelectricity of this compound below a first-order phase transition at 248 K is primarily due to the ordering of cations along a ferroelectric axis. In an intermediate phase between 248 and 233 K, the cation−anion sublattice displacement mechanism also gives a small positive contribution to ferroelectricity. In the family of the ferroelectric pyridinium salts, the paraelectric−ferroelectric phase transition temperature increases with the size and polarizability of the constituting anions, suggesting that the main interaction for ferroelectric ordering occurs via an indirect superexchange mechanism, whereas in compounds with small anions of low polarizability the direct dipole−dipole interaction dominates and leads to antiferroelectric order.

Introduction

The family of the pyridinium salts derived from strong inorganic acids is an excellent example for the study of orientational order as an origin of ferroelectricity. The majority of these salts are not ferroelectric and undergo a single order−disorder phase transition.[1,2] Ferroelectric salts in this family undergo a second and, some of them, a third phase transition within the ferroelectric phase.

$PyClO_4$ is a multidirectional ferroelectric salt with a first-order paraelectric−ferroelectric phase transition at 248 K. A further transition that takes place at 233 K is also of first order. The compound remains ferroelectric on further cooling. The detailed structure is available only for the high-temperature phase and was described by Czarnecki et al.[3] The symmetry of the high-temperature phase is R_{3m}. The elementary cell is near cubic, with coplanar pyridinium molecules at each corner and a perchlorate anion in the center. The body diagonal perpendicular to the cation plane is a 3-fold axis. In the intermediate phase, the crystal structure undergoes a subtle change, and the symmetry reduces to C_m. The low-temperature phase is believed to either remain C_m or to change to P_m.[3] $PyClO_4$ is isostructural at room temperature with pyridinium iodide, which does not show ferroelectric properties.[1]

The pyridinium ion is of C_{2v} symmetry, but due to the fact that carbon and nitrogen positions are not resolvable in X-ray analysis and that the C−N and C−C bond lengths are as well the same within experimental error,[3] its structure is akin to benzene, and a pseudo-C_6 axis can be assumed.

The perchlorate anion is strongly disordered at room temperature, and the positions of the oxygen atoms are not resolvable.[3] Its structure in this crystal is therefore not exactly known; however, it is tetrahedral in a vacuum and most likely also in the high-temperature phase. The possibility of distortion from tetrahedral symmetry in the intermediate and low-temperature phase will be discussed further as one of the possible reasons for the appearance of ferroelectricity.

In this study, it is verified that pyridinium cations rotate about the pseudo-C_6 axis of the pyridinium cation ring. The intention is to correlate the alignment of the cation permanent dipole moments with the observed macroscopic ferroelectricity and to discuss possible reasons for the appearance of ferroelectric polarization. The ^2H NMR technique is particularly suitable for the investigation of dynamics in molecular solids.[4] The paraelectric−ferroelectric phase transition temperatures in this family of pyridinium salts are compared, and the influence of the anions on the ferroelectricity is examined with the help of ab initio calculations. Factors influencing the appearance of ferroelectricity and the character of the phase transition are discussed as well.

Experimental Section

Materials. Pyridine-d_5 (99 atom % D) and perchloric acid were purchased from Aldrich Chemicals and used without further purification. Samples were prepared by crystallization from mixtures of the perdeuterated pyridine and perchloric acid from 80% ethanol/20% water solution.

DSC Measurements. A differential scanning calorimeter Netzsch DSC-204 was used to perform measurements on Py-d_5ClO_4 from 215 up to 290 K with a heating rate of 5 K min^{-1}.

NMR Experiments. ^2H NMR experiments were performed at 46.07 MHz on a Bruker CXP 300 spectrometer interfaced to a Tecmag spectrometer control system. ^2H NMR spectra were recorded with the quadrupole echo sequence $((\pi/2)_x - \tau_1 - (\pi/2)_y - \tau_2)$ with $\pi/2$ pulses of 2.2 μs and a pulse spacing of $\tau_1 = \tau_2 = 20$ μs. A modified inversion recovery sequence $((\pi/2)_\phi(\pi/2)_{(\phi\pm\pi/2)}(\pi/2)_\phi - \tau_r - (\pi/2)_x - \tau_1 - (\pi/2)_y - \tau_2$ with ($\phi = 0, \pi/2, \pi, 3\pi/2$)) was applied to determine spin−lattice relaxation times (T_{1Z}) and to record the corresponding partially relaxed spectra.[5] The recycle delay between successive scans was at least 10 times the spin−lattice relaxation time T_{1Z}. The number of scans was 16 or 32. The temperature of the sample

* Corresponding author. E-mail: e.roduner@ipc.uni-stuttgart.de.

10.1021/jp060502k CCC: $33.50
Published on Web 04/11/2006

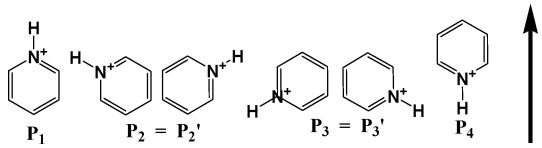

Figure 1. Orientations of the pyridinium cation and the corresponding populations with respect to the ferroelectric axis (indicated by the arrow).

was controlled with a Bruker BVT 1000 control unit, and in general, it was stable to within ±1 K. Measurements were done starting from room temperature and cooling in increments. After finishing the measurements at lower temperatures, the room-temperature measurement was repeated to check the reproducibility. Before each measurement, the sample was allowed to thermally equilibrate for 20−30 min.

NMR Data Processing, Simulations, and Analysis. Quantitative analysis of quadrupole echo and inversion recovery experiments provides detailed insight into the pyridinium cation dynamics as a function of temperature.[6,7] We used the in-plane six-site jump model described by Beck et al.[6] in the study of pyridinium tetrafluoroborate ($PyBF_4$). Orientations with respect to the ferroelectric axis and corresponding populations are defined in Figure 1. On the basis of the symmetry of the pyridinium cation and in agreement with earlier work, a six-site jump model appears as a realistic approximation for the cation reorientational motion.

The potential used for the six-site jump model is a superposition of a 6-fold potential due to the approximate cation symmetry and a 1-fold potential due to the ferroelectric field and is given by

$$V = \frac{V_1^0}{2}\sin\left(\Psi - \frac{\pi}{2}\right) + \frac{V_6^0}{2}\sin\left(6\Psi - \frac{\pi}{2}\right). \qquad (1)$$

Enthalpies obtained from DSC measurements are compared with the data obtained from the NMR data analysis. The latter are calculated from the populations derived from simulations of the quadrupole echo NMR experiments. For each fraction of molecules that changes orientation during incremental heating, it is possible to calculate the enthalpy increment by employing a formula that relates to the van't Hoff equation[6]

$$\Delta H_n = -f \times R\frac{\Delta(\ln K)}{\Delta(1/T)} \qquad (2)$$

where ΔH_n is the fractional enthalpy change between two successive temperature points, f represents a fraction of molecules that change orientation, and K are individual equilibrium constants for each jump reorientation.[6]

The macroscopic polarization in the model of Beck et al.[6] is calculated from the populations by using the formula:

$$\mathrm{pol}_{\mathrm{NMR}} = \frac{Z \times \mu_{\mathrm{cat.}} \times (p_1 + p_2 - p_3 - p_4)}{V_{\mathrm{cell}}(T)} \qquad (3)$$

where $\mu_{\mathrm{cat.}}$ is the dipole moment of the pyridinium cation, Z is the number of cations in the unit cell and $V_{\mathrm{cell}}(T)$ is the unit cell volume, which depends slightly on temperature.[8]

The pyroeffect measurements proved difficult due to the hygroscopic nature and experimental imperfections in the preparation of the $PyClO_4$ single crystal and in the pyroeffect measurements.[8,9] To circumvent the experimental uncertainties, we introduce the unit "% relative polarization". This is the fractional shift of the macroscopic polarization (NMR-derived and experimentally measured) between its lowest value (0% in the high-temperature phase) and its highest value (100% at the lowest temperature measured). In this way, we compare NMR-derived and experimentally measured macroscopic polarizations and avoid the uncertainty in the exact value of the dipole moment used for the translation of the NMR-derived populations into ferroelectric polarizations.[6,10]

TABLE 1: Constants Used in Simulations

parameter	value
quadrupolar coupling constant[a] (e^2qQ/h) (kHz)	179
transformation angles[b] (deg)	
ϕ	0
θ	90
ψ (deg)	±120; ±60, 0, +180
residual line width ($1/\pi T_2$) (kHz)	from 2.542 to 3.142

[a] Asymmetry parameter $\eta = 0$. [b] Euler angles ϕ, θ, and Ψ relating the magnetic principal axis system and the molecular axis system.

The normalized NMR derived results are compared in Figure 7 with the normalized data from pyroeffect measurements in the direction *parallel* to the 3-fold axis of the high-temperature phase.[8] The appearance of a polarization in this direction is explained by a flipping of the cations by 90° when a single crystal is pulled into the single ferroelectric domain during the course of the experiment. The flipping of cations would not change the symmetry group of the crystal.

Assuming that the difference between the measured pyroeffect and NMR-derived polarizations is due to an anion−cation sublattice displacement, it is possible to calculate the relative displacement x from

$$x = \frac{(\mathrm{pol}_{\mathrm{NMR}} - \mathrm{pol}_{\mathrm{pyro}})V_{\mathrm{UnitCell}}}{q} \times \frac{1}{3.336 \times 10^{-30}\,\mathrm{Cm}} \qquad (4)$$

where $\mathrm{pol}_{\mathrm{NMR}}$ and $\mathrm{pol}_{\mathrm{pyro}}$ are macroscopic polarizations derived from NMR and pyroeffect data, and q is the unit electric charge.[6]

To calculate the sublattice displacement, the NMR derived results were normalized to the absolute value of the highest and lowest experimentally measured macroscopic polarization and then used in the calculation.

The simulations of the quadrupole echo spectra were performed on the basis of the six-site jump model in the fast exchange limit and matched with experimental spectra by variation of the p_1 value. The populations p_2, p_3, and p_4 are related to p_1 by the 1-fold potential V_1^0.

Experimental spin−lattice relaxation times T_{1Z} were determined by analysis of the amplitudes of the experimental free induction decay (FID) from the inversion recovery experiments. Data processing was performed on a SUN workstation and a personal computer using the NMR1 and Sybyl/Triad software packages (Tripos, St. Louis, MO). Simulations were done by using an appropriate FORTRAN program[11] that describes the theoretical behavior of an $I = 1$ spin system during quadrupole echo and inversion recovery experiments, under the assumption that no other motion of the ring except rotation about the pseudo-C_6 axis takes place. Simulations of the experimental data from inversion recovery experiments were done on the basis of the 6-site jump model by varying the motional correlation time τ_c and by using the other parameters (populations p_1, etc.) deduced from the analysis of ^2H NMR quadrupole echo spectra. The constant parameters used during the present data analysis are summarized in Table 1.

Ab Initio Calculations. The calculations were performed for the anions in a vacuum by using the Gaussian 03 software package.[12] The implemented B3LYP functional and a 6-311++G**

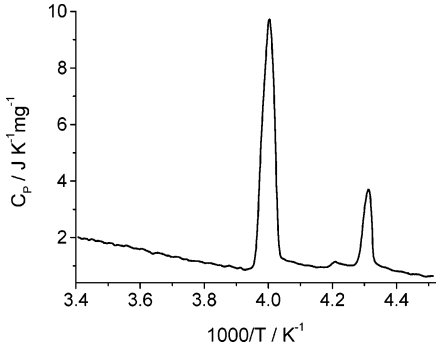

Figure 2. DSC measurements for $PyClO_4$-d_5 at a heating rate of 5 K min^{-1}, revealing $\Delta H_1 = 4.3$ kJ mol^{-1} and $\Delta H_2 = 0.8$ kJ mol^{-1} for the paraelectric−ferroelectric and the other solid−solid phase transition, respectively.

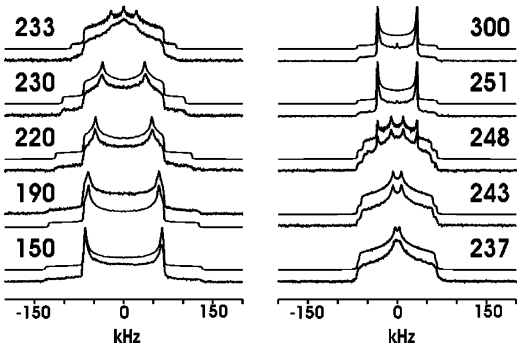

Figure 3. Experimental (lower) and simulated (upper, vertically displaced for clarity) ^{2}H NMR quadrupole echo spectra at selected temperatures. Temperatures in K are given above the corresponding spectra. Note the spectral superposition at the phase transition temperatures of 248 and 233 K.

basis set were used for B, F, P, Cl, O, and S atoms, and the LANL2DZ basis set for Cr. For I and Re atoms, the LANL2DZ ECP basis sets and potentials were used as described in other studies.[13,14] Anion polarizabilities were calculated on the basis of the previously optimized structures.

Results

DSC Measurements. From the DSC measurements shown in Figure 2, the phase transition enthalpies at 248 and 233 K are determined to be $\Delta H_1 = 4.3$ and $\Delta H_2 = 0.8$ kJ mol^{-1}, respectively. The very small peak between the phase transitions was not studied particularly because it showed a near-negligible heat effect (also noticed previously[8]) and did not lead to any observable effects in the NMR spectra.

NMR Experiments. In Figure 3, representative quadrupole echo ^{2}H NMR spectra are given along with the corresponding simulations. The phase transitions at 248 and 233 K have a great influence on the ^{2}H NMR line shapes. In the high-temperature phase, axially symmetric line shapes are detected. The splittings between the inner singularities in the low, intermediate, and high-temperature phase, here denoted as Δ_1, Δ_2, and Δ_3, respectively, are given in Table 2. In the high-temperature phase, the observed splitting is compatible with a highly symmetric, fast uniaxial rotational jump process about an axis perpendicular to the molecular plane, and the splitting does not depend significantly on temperature. However, in the intermediate- and low-temperature phases, the splitting varies considerably with temperature. Here, typical nonaxially symmetric ^{2}H NMR spectra are observed, reflecting the presence of hindered overall motions of lower symmetry. At the lowest temperature, again, an almost axially symmetric ^{2}H NMR spectrum with a splitting

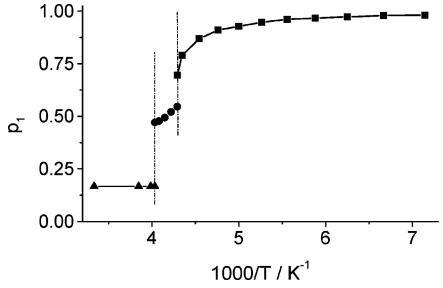

Figure 4. Temperature dependence of the population p_1. Vertical lines represent the reported phase transition temperatures.[3]

TABLE 2: Experimental Splittings between Singularities Obtained Both from Quadrupole Echo and Partial Recovery Spectra with Longest Delay

T/K	Δ_1/Hz	Δ_2/Hz	Δ_3/Hz
140	128688		
150	128508		
160	125890		
170	124299		
180	122881		
190	118736		
200	112653		
210	107574		
220	95351		
230	71377		
233	42508	0	
237		7184	
239		10206	
241		14195	
243		14753	
245		15982	
245		18149	
248		20409	66552
251			66226
260			66030
270			65981
290			65710
300			66030

characteristic for the rigid limit case is observed. Variable-temperature ^{2}H NMR spectra recorded for the N-deuterated pyridinium perchlorate (spectra not shown here) gave identical spectra, confirming that there is no other motion except the one about the pseudo-C_6 axis. A coexistence of two phases is clearly observed in the spectra at both phase transition temperatures, as expected for first-order transitions.

The temperature dependence of the p_1 values is given in Figure 4. In the high-temperature phase, the population amounts to 0.1667, demonstrating six equally populated orientations, while in the intermediate- and low-temperature phase, p_1 increases at the cost of p_2, p_3, and p_4, indicating that the degeneracy of the six orientations is lifted. At both phase transitions, a discontinuous change of p_1 is observed, indicating again that they are of first order.

Selected experimental partially relaxed ^{2}H NMR spectra from the inversion recovery experiment, along with the corresponding simulations, are given in Figure 5. Simulations on the basis of the six-site jump model match the experimental spectra quite well at 255 K, with small differences at intermediate delay times at the lowest temperatures. The corresponding experimental and simulation-based T_{1Z} values are displayed in Figure 6. The two sets of data mostly agree within error.

Ferroelectric Polarization. The macroscopic ferroelectric polarization is calculated based on eq 3 and then presented in % polarization, as described in the experimental part (Figure 7). The populations are derived from the ^{2}H NMR data analysis, and the unit cell volume as a function of temperature was

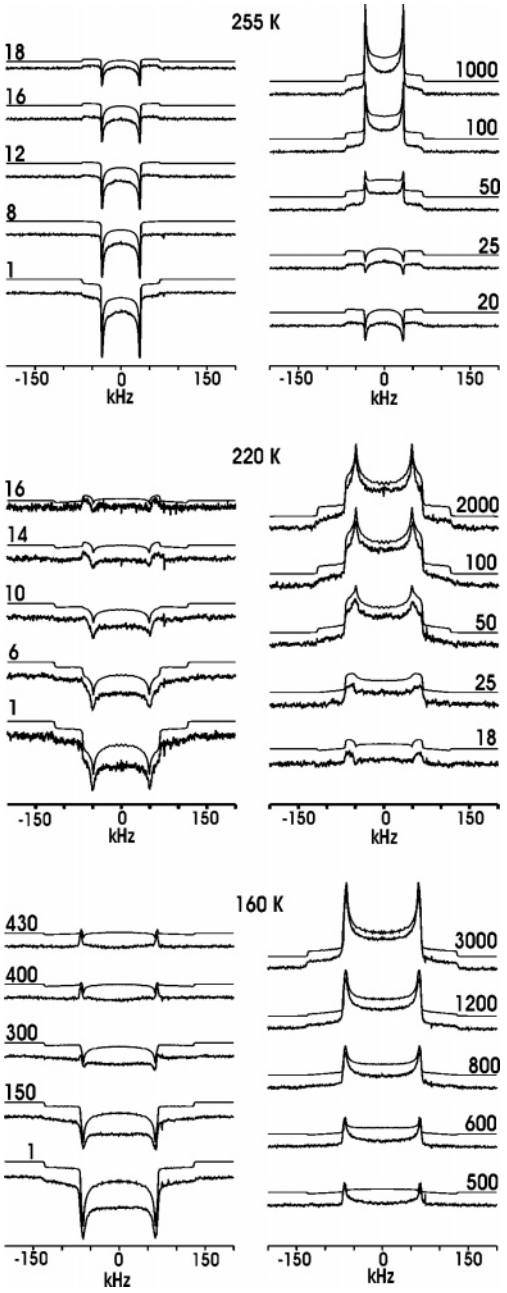

Figure 5. Experimental (lower) and simulated (upper, vertically displaced) partially relaxed ^{2}H NMR spectra (inversion recovery experiment) at selected temperatures with relaxation delays τ_r in milliseconds.

determined in dilatometric experiments by Szafraniak at al.[8] The number of ion pairs in the unit cell remains 3 in all phases.

In the *low-temperature* range, the agreement between the results obtained on the basis of the NMR data analysis and those from pyroeffect measurements is nearly perfect because of the intentional matching of the low-temperature end of the curves. Small deviations may be attributed to experimental imperfections. In contrast, in the *intermediate-temperature* phase, the deviations are too high to be explained by experimental errors. Obviously, there must be an additional mechanism that contributes to ferroelectricity.

Ab Initio Calculations. The results of the ab initio calculations are presented in Table 3. They show that the anion polarizability increases with the anion volume, as revealed by the corresponding bond lengths. Primarily, this is due to the higher polarizability of the central atom because of its larger

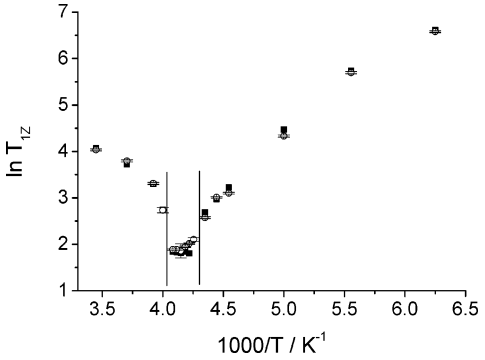

Figure 6. Experimental (open circles with error bars) and simulation-based (solid squares) T_{1Z} relaxation times. The vertical lines represent the phase transition temperatures.

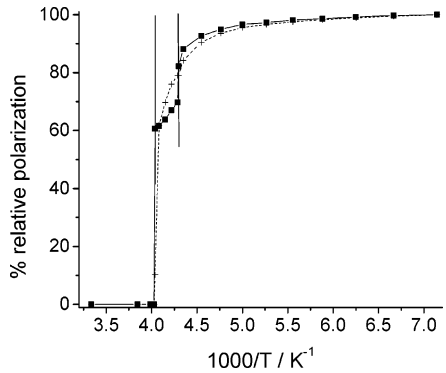

Figure 7. Relative polarization from pyroeffect measurements in the direction parallel to the 3-fold axis (crosses) and derived from NMR populations (squares). Vertical lines represent the phase transition temperatures.

number of electrons. The partial charges on the anion's peripheral atoms obey the same trend, with the exception of the case of ReO_4^-, where the outer atoms have a much larger negative partial charge than expected from the trend of unit cell volume per number of ions.

Discussion

Possible candidates for the difference between the macroscopic ferroelectric polarizations and the ones derived from NMR (Figure 7), which will be discussed in the following, are: (i) the cation−anion sublattice displacement, as suggested earlier for $PyBF_4$,[6] (ii) a displacement of the cation center of charge out of the cation center of mass when the cation rotation slows down, and (iii) the presence of a dipole moment of the anion when it is distorted from tetrahedral symmetry.

(i) If sublattice displacement takes place, then values of up to −0.12 Å in the intermediate-temperature (positive contribution to the macroscopic polarization) and of up to +0.04 Å in the low-temperature phase, as displayed in Figure 8, are required to explain the difference between macroscopic and NMR-derived ferroelectric polarization.

(ii) Another possible contribution to the ferroelectric polarization in the intermediate-temperature phase may arise from the fact that the center of charge of the pyridinium ion is at a slightly different position than the center of mass. This effect becomes important when the rotational jump process is slowed in the intermediate-temperature and, especially, in the low-temperature phase. In this respect, $PyClO_4$ should be similar to $PyBF_4$, where the contribution to ferroelectric polarization was found to be less than 2%.[6]

(iii) The comparison between all pyridinium salts reveals that the ferroelectric ones have anions with tetrahedral structure in

TABLE 3: Properties of the Anions Derived from Ab Initio Calculations[a]

anion	ordering temperature/K	$\alpha^b/10^{-30}$ m^{-3}	dipole moment/D	atom−atom pair	bond lengths/Å	partial atomic charges/e
BF_4^-	240 (fe)	3.05557	/	B−F	1.4173	B (+1.066) F (−0.516)
ClO_4^-	248 (fe)	5.59397	/	Cl−O	1.5006	Cl (+0.235) O (−0.309)
FSO_3^-	282 (fe)	5.12571	0.3713	S−F	1.5290[c]	S (+0.558) F (−0.332) O (−0.409)
$FCrO_3^-$	258 (fe)	6.00148	0.1889	Cr−O	1.6500[c]	O (−0.499) F (−0.546) Cr (+0.042)
ReO_4^-	333 (fe)	7.88491	/	Re−O	1.74346	Re (+2.203) O (−0.800)
IO_4^-	321 (fe)	8.69548	/	I−O	1.80181	I (+1.235) O (−0.559)
Cl^-	∼340 (afe)	2.34393	/	/	/	−1
Br^-	270 (afe)	3.76734	/	/	/	−1
I^-	249 (afe)	9.52051	/	/	/	−1
PF_6^-	217 (afe)	3.83841	/	P−F	1.64555	P (+0.612) F (−0.227)

[a] fe: paraelectric−ferroelectric; afe: paraelectric−antiferroelectric. [b] Isotropic value for a static electric field. [c] Mean distance between central and all outer atoms.

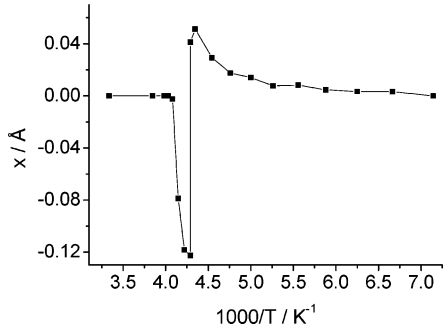

Figure 8. Sublattices displacement calculated from the difference of NMR (using a dipole moment of 1.97 D) and pyroeffect data. Vertical lines represent the phase transition temperatures.

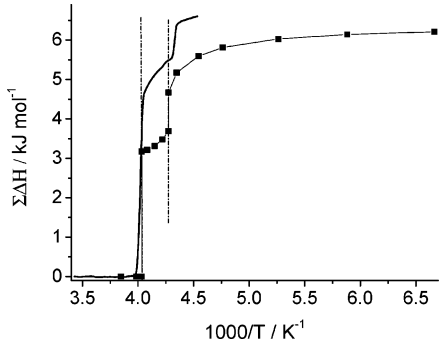

Figure 9. Total change of enthalpy from NMR data (squares) and DSC measurements (full line). The two data sets are matched in the high-temperature phase. Vertical lines represent the phase transition temperatures.

a vacuum ($PyClO_4$,[3] $PyBF_4$,[6] $PyIO_4$,[10,15] $PyReO_4$ [16]) or are of pseudotetrahedral symmetry ($PyFCrO_3$,[17] $PyFSO_3$ [18]), while others, like PyI,[2] PyBr,[2] and $PyPF_6$,[19] are not ferroelectric. In the crystal, the tetrahedral symmetry of the free anion can be lowered toward C_{3v} or D_{2d}. Lowering toward C_{3v} would create a dipole moment. Distortion from tetrahedral symmetry in the crystal lattice has been observed in a neutron diffraction study of $PyIO_4$, resulting in a dipole moment of 0.27 D,[15] and for guanidinium perchlorate, where one of the bonds was found to be stretched by 0.05 Å.[20] If the same distortion would take place for $PyClO_4$, then the dipole moment of the anion would contribute significantly to the polarization both in the intermediate and in the low-temperature phases. Unfortunately, it is not known whether there is such a distortion in the ferroelectric phases.

It is therefore concluded that the cation−anion sublattices' relative displacement is the most likely explanation for the difference, shown in Figure 7, between the macroscopic and the NMR data sets in the intermediate-temperature phase. In contrast to the case of $PyBF_4$, [6] this displacement gives a positive contribution to the macroscopically observed polarization and builds up crystal strain as well. Figure 8 shows that this strain is released at the second phase transition at 233 K.

The ratios of the NMR-derived results at the para-to-ferroelectric phase transition temperature and at the lowest temperature match almost quantitatively the ratio of the experimentally measured results, once again confirming that ferroelectricity in this ferroelectric salt is of order−disorder type.

For a test, eq 3 can also be used for the calculation of the limiting value of the polarization of $PyIO_4$, assuming full ordering of all cations ($p_1 = 1$), neglecting the fact that they are tilted with respect to the ferroelectric axis. After introducing the other constants ($Z = 4$, $V = 751$ Å^3, $\mu = 1.97$ D)[10] a spontaneous polarization of 3.45 μC cm^{-2} is obtained, somewhat less than the reported experimental value at the lowest temperature ($T = 120$ K) of 3.95 μC cm^{-2},[10] despite the neglected tilt. While this confirms that the present model can predict *absolute* polarizations, it also means that an additional mechanism contributes to the polarization of $PyIO_4$.

Heat Content. Comparison of the enthalpies derived from the NMR measurements (eq 2) with those measured by DSC shows a difference of approximately 10%, depending on the actual sample temperature (see Figure 9). The integrated enthalpy changes measured by DSC depend somewhat on the choice of baseline and the range of measurements. However, even here, exactly the same trends are observed in the change of the calorimetric and the NMR-derived integrated enthalpy, implying that the model used here is appropriate. This means that most of the energy released during cooling originates from

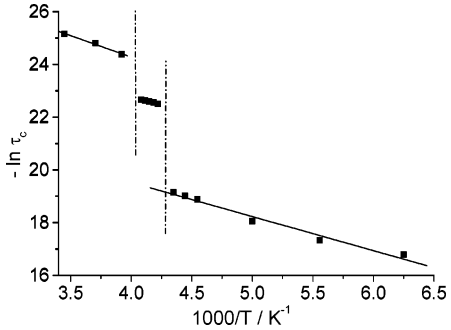

Figure 10. Arrhenius plot of the correlation time τ_c derived from simulations of the T_{1Z} relaxation data. Vertical lines represent the phase transition temperatures.

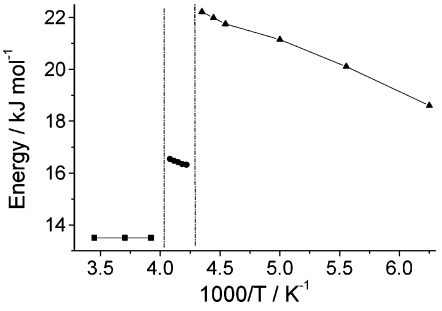

Figure 11. Activation energies using the frequency factor of the high-temperature phase (see text). Vertical lines represent the phase transition temperatures.

the ordering of pyridinium cations. The difference between the two curves corresponds to the heat released by other possible processes (ordering of anions, structural change, etc.). The enthalpy change at the higher-temperature phase transition measured by DSC is higher by about 44% than the one calculated from the NMR measurements, suggesting that a significant portion of the energy is released in other processes, probably by spring-loading the lattice as in $PyBF_4$.[6] At the low-temperature phase transition, the difference is approximately 9%. In this case, the structural change is of minor importance, and the released energy arises almost completely from the ordering of the pyridinium cations.

Dynamic Properties. The motional correlation time τ_c for the pyridinium rotational jumps derived from the inversion recovery experiments are plotted against the inverse temperature in Figure 10. They clearly follow Arrhenius behavior in all three phases. The apparent activation energies for the high-, intermediate-, and low-temperature phases amount to 13.5, 7.4, and 6.4 kJ mol^{-1}, respectively. The values for the high-temperature phase is lower than those reported for pyridinium iodide, pyridinium tetrafluoroborate, and pure solid benzene.[1,6,21,22] The corresponding preexponential factors are 2.32×10^{13}, 6.96×10^{11}, and 5.3×10^{10} s^{-1} for the high-, intermediate- and low-temperature phases, respectively.

To judge these values, we estimate the preexponential factor, assuming that it is the attempt frequency to cross the energy barrier in the forward or backward direction, which is given by twice the frequency of the cations' vibrational oscillation frequency. In the high-temperature phase, rotational jumps occur between degenerate 6-fold potential wells, the 1-fold potential being zero (eq 1). The harmonic force constant for the oscillating motion is then given by the second derivative at the potential minimum, $k = 18V_6^0 = 243$ kJ mol^{-1}. Thus, the frequency of the cation librational motion with moment of inertia I amounts to $\nu = (k/4\pi^2 I)^{1/2} = 0.93 \times 10^{12}$ s^{-1} (62.24 cm^{-1}). This translates into an attempt frequency of 1.87×10^{12} s^{-1} in the ground state and 1.25×10^{13} s^{-1} in the Boltzmann average at 298 K, which is in near quantitative agreement with the observed Arrhenius preexponential factor. The remaining factor of 1.8 may be due to the fact that the actual potential is of a cosine rather than the assumed parabolic (harmonic) shape. According to our knowledge, the vibrational frequency has not yet been measured for this compound.

Because the crystal is more densely packed at lower temperatures, it seems unreasonable that the activation energies are lower for the intermediate- and low-temperature phases. Furthermore, the preexponential factor should be expected to stay roughly constant. The discrepancy between expectation and observation suggests the presence of an additional process that affects the apparent Arrhenius parameters. We suggest that this is due to the increasing 1-fold potential, arising form the build up of ferroelectricity with decreasing temperature. It adds increasingly to the activation energy and pretends a different Arrhenius behavior. On the basis of this assumption, we fixed the frequency factor at its high-temperature value and calculated the activation energy for each temperature point. The values derived are displayed in Figure 11. They now show the expected *increase* to ca. 16 and 22 kJ mol^{-1} over the two phase transitions toward the lower temperatures, but within the intermediate- and lower-temperature phases, the activation energies still decrease slightly with decreasing temperature. Constant or moderately increasing activation energies would require increasing preexponential factors with decreasing temperature, which may be possible when the effect of the increase of V_1 is stronger than that of the decreasing Boltzmann term.

Comparison with Other Ferroelectric Pyridinium Salts. In this family of ferroelectric compounds, the "carriers" of the ferroelectricity are the pyridinium cation electric dipole moments, but the "governors" of the phase transition temperatures are the anions, because the cations are always the same.

Figure 12a shows that the paraelectric−ferroelectric phase transition temperature *increases* with the unit cell volume per number of ion pairs. The trend is not linear and shows deviations for FSO_3^- and ReO_4^-. For the case of FSO_3^-, it is conceivable that this is due to the presence of a significant dipole moment of the anion, as seen in Table 3. At first sight, such an increase with specific unit cell volume is unexpected. For the more voluminous anions, the distance between pyridinium dipoles is larger, thus decreasing the direct electrostatic dipole−dipole interaction energy, which can be balanced by thermal energy already at lower temperature so that the phase transition temperature should be expected to increase with *decreasing* unit cell volume. This is compatible with the reported increase of transition temperatures under external pressure,[3] but not with the unit cell volume as a function of anion size.

In the case of $PyClO_4$, $PyBF_4$, and $PyFSO_3$ sheets of coplanar cations are sandwiched between sheets of anions, and the anion diameter determines the distance between the cation sheets. In the other cases, the cations are slightly tilted, but the diameter of the anion still determines the distance between the cation sheets. The two-dimensional periodic structure with cation dipoles at the corners of equilateral triangles within one sheet is an arrangement of relatively low ferroelectric dipolar interaction energy, which in the average between one dipole and its six nearest neighbors amounts to only 12.5% of its maximum possible value of one pair. In this situation, it is conceivable that the coupling in the third dimension, between neighboring cation sheets, is of crucial importance. The interspersed anions take a special role because they determine the distance between the cation sheets. Moreover, they play a more active role due

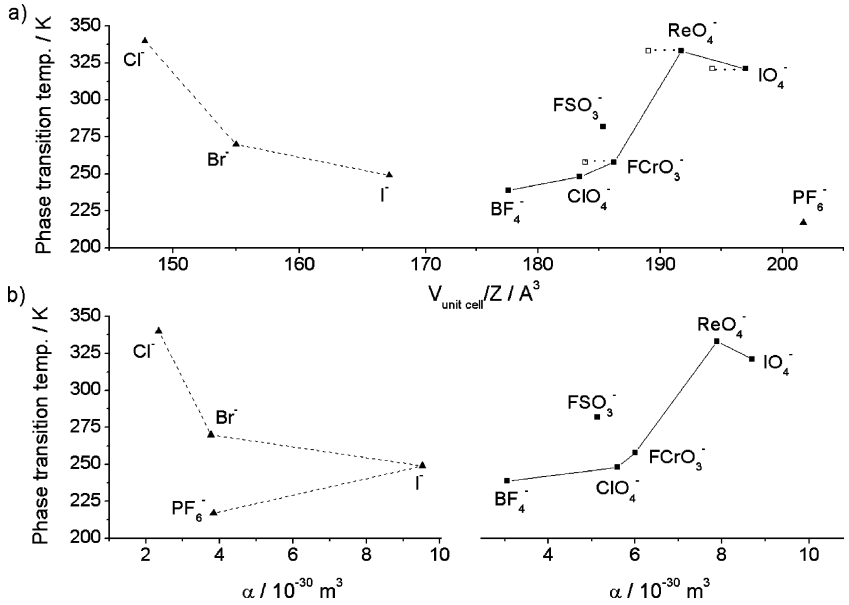

Figure 12. (a) Order−disorder phase transition temperature vs unit cell volume of the high-temperature phase for antiferroelectric (▲) and ferroelectric (■) pyridinium salts. Where known, the unit cell volume is also given for the phase below the ordering transition (○). (b) Order−disorder phase transition temperature vs polarizability of the anion for anitferroelectric (left) and ferroelectric salts (right).

to their polarizability, which provides an indirect "superexchange" coupling between the cation dipoles.

When the cations are tilted, this decreases the dipole−dipole interaction so that one should expect the ordering phase transition to occur at lower temperatures, which disagrees again with the experimental observations. The intermediate (ferroelectric) phase of $PyReO_4$, $PyIO_4$, and $PyFCrO_3$ is orthorhombic (still with noncoplanar cations). Despite these structural differences, we have a systematic trend, but these differences are probably responsible for the scatter in Figure 12a (right-hand side).

The unit cell volumes in Figure 12a are available for the paraelectric high-temperature phases because the structures of the intermediate phases are often not known, but for some of the compounds, this information is available and given by an open symbol connected by a dotted line. It can be seen that these show the same trend.

For a more precise discussion, anions should not be viewed as point charges, and cation dipole moments not as point dipoles, because the distances between them are very small. In all compounds, the anions consist of a varying inner atom and of outer atoms that are almost exclusively oxygen atoms. Their partial charges, which are given in Table 3, dominate the electrostatic interaction.

The anions are positioned more or less symmetrically about the cation. If the situation remains the same in the intermediate-temperature phase, then the interaction of the positive end of a cation dipole is always balanced by that of the negative end, and there is no net contribution of the anion to ordering. In the case of ReO_4^-, the large deviation from the overall trend may be related to the very large partial charge of its outer atoms.

A plausible explanation for the trend displayed in Figure 12 results from induced rather than permanent charges. This is demonstrated in Figure 12b (right-hand side), which shows that the anion polarizability α exhibits a quite similar behavior as a function of phase transition temperature as the unit cell volume. Anion polarization stabilizes both ends of a cation dipole and provides a superexchange mechanism that stabilizes both the ferroelectric and, probably, to a lesser extent the antiferroelectric phases, so that the transition temperature in compounds with highly polarizable anions is higher.

Comparison with Nonferroelectric Pyridinium Salts. The high-temperature phase of all pyridinium salts is found to be disordered. By comparing the nonferroelectric compounds PyCl, PyBr, PyI, and $PyPF_6$, [2] and the ferroelectric salts (Table 3), we see that, with the exception of $PyPF_6$, the ferroelectric ones have a much larger unit cell volume due to the larger anion diameters, resulting in a better separation of the cation layers. In fact, unlike for the ferroelectric compounds, among these nonferroelectric salts,[2] the phase transition temperature *decreases* with increasing anion radius (Figure 12a, left-hand side). An ordered antiferroelectric arrangement was observed in the low-temperature phase of PyCl,[23] and the same has been suggested for other PyX salts as well (X = Br, I, and PF_6).[2]

The different behavior may be explained in the following way. When the cation sheets are separated above a certain distance, determined by the anion radius, the superexchange interaction among cations dominates and causes ferroelectric ordering. For the smaller anions, the superexchange interaction between cation sheets is decreased. In this case, the energetically favored arrangement is antiferroelectric where cation sheets interact directly. The small anions have small polarizabilities as well, as seen in Figure 12b, left-hand side. $PyPF_6$ represents an exception from this behavior. This anion is large (Figure 12a, right-hand side), but it has a relatively small polarizability (Table 3 and Figure 12b, left-hand side) due to the compact nature of the fluorine atoms. The partial charge on its peripheral atoms is the smallest among all pyridinium salts examined here.

As can be seen in these graphs, PyI and $PyBF_4$ are the borderline cases. I^- has a large polarizability, but the distance between sheets is too small, and BF_4^- has a relatively small polarizability, but the distance between sheets is large, confirming that the distance between the cation sheets plays an important role.

For $PyFCrO_3$ and $PyReO_4$, the high-temperature phase is paraelectric, the intermediate one is ferroelectric, but the order of the low-temperature phase is antiferroelectric. This demonstrates that the behavior of pyridinium salts is influenced by a delicate balance of numerous factors.

Phase Transition Order. $PyClO_4$ has two first-order phase transitions, $PyReO_4$ and $PyIO_4$ have second-order transitions, while $PyBF_4$ is a limiting case,[6] and for the other compounds, the phase transition order is not known. What influences the character of the phase transition is not clear. It was previously suggested that, with raising an applied pressure on PyI, PyBr, and other PyX salts, the phase transition would change to second order.[2] This is due to the disappearance of the phase transition volume change (which is typical for second-order transitions) with increasing external pressure, which has a similar effect as a chemical pressure. Chemical pressure arises due to a reduced anion radius and a smaller distance between the cation sheets.[2] The pyridinium rings of ferroelectric $PyClO_4$ and $PyBF_4$ in the high- and in the intermediate-temperature phases are coplanar, and the structural changes are known to be minimal. The cations in $PyReO_4$ and $PyIO_4$ are noncoplanar (tilted), and the paraelectric−ferroelectric phase transition is of second order. An arrangement where the positive partial charge of the pyridinium ring is directed toward the negative charge of the neighboring pyridinium ring is energetically favored.

It seems that the phase transition character is determined by the internal pressure in the crystal and the packing of the pyridinium rings as well. Better-packed crystals (canted cations) require smaller structural rearrangement, and the phase transition is of second order.

Conclusions

The ^2H NMR data (quadrupole echo and inversion recovery experiments) of $PyClO_4$ can be quantitatively reproduced on the basis of a rotational jump motion of the pyridinium cations about their pseudo-C_6 axes. The high-temperature phase above 248 K is fully disordered, and the pyridinium cations undergo fast jumps between equally populated sites. In the intermediate- and low-temperature phases, motion occurs between unequally populated sites and results in domains of almost completely static and fully aligned cations near 140 K. The intermediate-temperature phase can still be considered as disordered, but the reorientation of the pyridinium cations occurs in a way that the average dipole moment along the ferroelectric axis is nonzero, giving rise to temperature-dependent domain polarization. Sublattice displacement gives an additional small positive contribution to the macroscopically observed polarization in this phase.

Heat released during cooling originates mainly from the ordering of cation dipole moments. The difference between the heat released at the phase transitions and the heat necessary for ordering of the cations, appearing mainly at the higher phase transition, is attributed to other possible processes such as spring-loading the lattice or anion ordering.

The high polarizability of large anions is suggested to be a key property that is responsible for ferroelectric ordering by an *indirect* mechanism via superexchange, whereas compounds with small anions in which the *direct* cation dipole−dipole interaction dominates become antiferroelectric. This is revealed by correlations of the ordering phase transition temperatures with the anion polarizability and the anion size.

Acknowledgment. We thank Dr. habil. Piotr Czarnecki and Isabella Szafraniak for giving us the results of the pyroeffect and the volume measurements.[8,9] Helpful discussions with Prof. Thomas Schleid and Dr. Bettina Beck on this subject as well as support by Drs. Thomas Handel and Jorge Garibay during NMR experiments are gratefully acknowledged. We thank the Deutsche Forschungsgemeinschaft for financial support within the Graduiertenkolleg Nr. 448 (Advanced Magnetic Resonance Type Methods in Materials Science).

References and Notes

(1) Ripmeester, J. A. *Can. J. Chem.* **1976**, *54*, 3453.
(2) Szafranski, M.; Szafraniak, I. *J. Phys.: Condens. Matter* **2003**, *15*, 5933, and references therein.
(3) Czarnecki, P.; Wasicki, J.; Pajak, Z.; Goc, R.; Maluszynska, H.; Habrylo, S. *J. Mol. Struct.* **1997**, *404*, 175.
(4) *Solid State NMR for Chemists*; Fyfe, C. A., Ed.; C.F.C. Press: Ontario, Canada, 1983.
(5) Heaton, N. J.; Vold, R. R.; Vold, R. L. *J. Magn. Res.* **1988**, *77*, 572.
(6) Beck, B.; Villanueva-Garibay, J. A.; Müller, K.; Roduner, E. *Chem. Mater.* **2003**, *15*, 1739.
(7) Fojud, Z.; Goc, R.; Jurga, S.; Kozak, A.; Wasicki, J. *Mol. Phys.* **2003**, *101*, 1469.
(8) Szafraniak, I.; Czarnecki, P. *J. Phys.: Condens. Matter* **2002**, *14*, 3321.
(9) Czarnecki, P. personal communication.
(10) Maluszynska, H.; Scherf, C.; Czarnecki, P.; Cousson, A. *J. Phys.: Condens. Matter* **2003**, *15*, 5663.
(11) Schmieder, J.; Müller, K. *J. Phys. Chem. A* **1998**, *102*, 1181.
(12) Frisch, M. J.; Trucks, G. W.; Schlegel, H. B.; Scuseria, G. E.; Robb, M. A.; Cheeseman, J. R.; Montgomery, J. A., Jr.; Vreven, T.; Kudin, K. N.; Burant, J. C.; Millam, J. M.; Iyengar, S. S.; Tomasi, J.; Barone, V.; Mennucci, B.; Cossi, M.; Scalmani, G.; Rega, N.; Petersson, G. A.; Nakatsuji, H.; Hada, M.; Ehara, M.; Toyota, K.; Fukuda, R.; Hasegawa, J.; Ishida, M.; Nakajima, T.; Honda, Y.; Kitao, O.; Nakai, H.; Klene, M.; Li, X.; Knox, J. E.; Hratchian, H. P.; Cross, J. B.; Bakken, V.; Adamo, C.; Jaramillo, J.; Gomperts, R.; Stratmann, R. E.; Yazyev, O.; Austin, A. J.; Cammi, R.; Pomelli, C.; Ochterski, J. W.; Ayala, P. Y.; Morokuma, K.; Voth, G. A.; Salvador, P.; Dannenberg, J. J.; Zakrzewski, V. G.; Dapprich, S.; Daniels, A. D.; Strain, M. C.; Farkas, O.; Malick, D. K.; Rabuck, A. D.; Raghavachari, K.; Foresman, J. B.; Ortiz, J. V.; Cui, Q.; Baboul, A. G.; Clifford, S.; Cioslowski, J.; Stefanov, B. B.; Liu, G.; Liashenko, A.; Piskorz, P.; Komaromi, I.; Martin, R. L.; Fox, D. J.; Keith, T.; Al-Laham, M. A.; Peng, C. Y.; Nanayakkara, A.; Challacombe, M.; Gill, P. M. W.; Johnson, B.; Chen, W.; Wong, M. W.; Gonzalez, C.; Pople, J. A. *Gaussian 03*, revision B.04; Gaussian, Inc.: Wallingford, CT, 2004.
(13) Hay, R. J.; Wadr, W. R. *J. Chem. Phys.* **1985**, *82*, 270.
(14) Hay, R. J.; Wadr, W. R. *J. Chem. Phys.* **1985**, *82*, 284.
(15) Maluszynska, H.; Czarnecki, P.; Lewicki, S.; Wasicki, J.; Gdaniec, M. *J. Phys.: Condens. Matter* **2001**, *13*, 11053.
(16) Wasicki, J.; Czarnecki, P.; Pajak, Z.; Nawrocik, W.; Szczepanski, W. *J. Chem. Phys.* **1997**, *107*, 576.
(17) Pajak, Z.; Maluszynska, H.; Szafranska, B.; Czarnecki, P. *J. Chem. Phys.* **2002**, *117*, 5303.
(18) Pajak, Z.; Czarnecki, P.; Maluszynska, H.; Szafranska, B. *J. Chem. Phys.* **2000**, *113*, 848.
(19) Wasicki, J. W.; Kozak, A.; Pajak, Z.; Czarnecki, P.; Belushkin, A. V.; Adams, M. A. *J. Chem. Phys.* **1996**, *105*, 9470.
(20) Pajak, Z.; Grottel, M.; Koziol, A. *J. Chem. Soc., Faraday Trans.* 2 **1982**, *78*, 1529.
(21) Wasicki, J.; Pajak, Z.; Kozak, A. *Z. Naturforsch. A: Phys. Sci.* **1990**, *45*, 33.
(22) Ok, J. H.; Vold, R. R.; Vold, R. L.; Etter, M. C. *J. Phys. Chem.* **1989**, *93*, 7618.
(23) Rerat, P. C. *Acta Crystallogr.* **1962**, *15*, 427.